First-principles modelling of stability of Ti_3Nb

Petr Lazar, Michal Jahnatek, Claudia Blaas-Schenner, Ryoji Asahi, and Jürgen Hafner
Institute of Physical Chemistry, University of Vienna, Sensengasse, 8/7, Wien, A1090, Austria.
(Dated: October 18, 2010)

We present a first principles study of ground-state and dynamical stability of austenite and martensite phase in binary Ti_3Nb, used as a model system for Gum Metal. We show that G1-type structure, recently proposed for high temperature austenite phase, is dynamically unstable within harmonic approximation, nevertheless anharmonic phonon-phonon interactions introduced by means of the self-consistent ab initio lattice dynamical method (SCAILD) stabilize the G1 structure at room temperature. The DO_3 structure is dynamically unstable from $T = OK$ up to $T = 1200K$ and anharmonic effects are not sufficient to stabilize the DO_3 structure. We evaluted relative stability of many hexagonal structures by performing a search over different possible distributions of Ti and Nb atoms in a hexagonal B_h lattice. In the case of α'' martensite we relaxed lattice parameters of the orthorhombic structure. For both stable martensites and G1 structure we used calculated phonon dispersions to evalute the vibrational contribution to the free energy and we estimated martensitic temperatures by comparing Helmholtz free energies as functions of the temperature.

PACS numbers: 61.50.Ah, 61.50.Ks, 62.50.+p, 62.20.Qp

INTRODUCTION

In spite of six decades of research, the underlying micromechanisms of deformation of titanium alloys, with their diversity of martensite phases and single-crystal behaviour, are still not well understood. In past several years, gum metals, a group of the least stable β titanium alloys, have been developed for their advantages of multifunctional properties after severe cold deformation. After severe cold swaging these alloys exhibit super-properties such as ultralow elastic modulus, superelasticity, ultrahigh strength, superplasticity and greatly reduced thermal expansion. The above unique properties are attributed to the lack of conventional dislocations, deformation twins and stress-induced martensitic transformation. Saito et al. [1] suggested that the unique properties are produced by a dislocation-free plastic deformation mechanism called giant planar faults, which induce crystallographic rotations from the neighboring area by plastic deformation. The calculations of Li et al. [2] supported the concept that the triggering stress for dislocation motion exceeded the ideal strength of gum metal. This could result in the plastic deformation through the giant planar faults accompanied by nanodisturbances, a kind of nanoscale dipoles of nonconventional partial dislocations with arbitrary and nonquantized Burgers vectors. However, recent work has shown that more conventional deformation mechanisms are still operative in the gum metals, for example, largely reversible stress-induced phase transformation during tensile loading and unloading was observed using in situ synchrotron x-ray diffraction. [3]

A stress-induced martensitic transformation to the orthorhombic α'' phase that is found in a number of Ti alloys. An early, partially reversible transformation to α'' would also introduce a pseudo-elastic deformation that would help to explain the low tensile modulus and large elastic deformation of the alloy. Previous investigations also showed compressional tension asymmetry for the martensitic transformation. That is, the α'' martensite can be detected by X-ray diffraction after compression but is barely detectable after tensile test, even on the tensile fracture surface. This evidence suggests that the multifunctional properties of Gum Metal may be attainable if the valence electron number e/a is slightly lower than 4.24 and the stress-induced martensitic transformation may take place in compression. [4]

Generally, the deformation behaviors of metastable β titanium alloys are closely related to the stability of β phase. The plastic deformation mode changes from the stress-induced martensite to twin or slip mechanism as the stability of the β phase increases. However, the boundaries between different mechanisms and the role of various elements in stabilization of β phase in Gum Metal are not quite clear.

Therefore, our calculations were aimed to reveal relative stability of high-temperature cubic β phase and martensitic phases in Ti_3Nb system. For β phase, we follow recent study by Nagasako et al. [5], which revealed that the DO_3 structure, which has been used as an approximant for studying binary Gum Metal, is inadequate due to its instability against shear deformations and the formation of vacancies and antisite point defects. Searching for a better structural model of Ti-Nb alloy at a A_3B stoichiometry, Nagasako et al. [5] performed supercell based search over many different possible distributions of Ti and Nb atoms in a B32 lattice and found that structures from the energetically most favorable symmetry equivalent group G1 are elastically stable and their shear moduli agree very well with those measured for Gum Metal, making the ordered binary alloy of the G1-type a good model system for studying the properties of Gum Metal. We will show that G1 structure phase is dynamically unstable in harmonic approximation, having imaginary frequencies of some optical phonon branches and that anharmonic phonon-phonon interactions are needed for its stabilization. As a result, phonon frequencies are temperature dependent and real eigen-frequencies of all phonon modes are found already at room temperature.

For martensitic phases, we evaluted relative stability of

many hexagonal structures by performing a search over different possible distributions of Ti and Nb atoms in a hexagonal B_h lattice. We have performed a complete relaxation of the volume and shape of the supercell and also of all atomic coordinates. For the energetically most favorable configurations we calculating their phonon dispersions using density functional perturbation theory within harmonic approximation. We found that dynamically stable configuration has monoclinically distorted hexagonal cell and is energetically more favorable than the G1 structure. In the case of orthorhombic α'' martensite we relaxed lattice parameters of the structure described in the literature [6]. For both stable martensites and G1 structure we used calculated phonon dispersions to evalute the vibrational contribution to the free energy and we estimated martensitic temperatures by comparing Helmholtz free energies as functions of the temperature.

COMPUTATIONAL DETAILS

The DFT calculations have been performed by application of the Vienna *ab initio* Simulation Package (VASP).[7, 8] We used the projector augment wave (PAW) method with the generalized gradient approximation according to the parameterization of Perdew and Wang.[9] Convergency of the total energies with respect to basis size and number of **k** points for the Brillouin zone integration was carefully checked. The PAW potentials were used with energy cutoffs of 300 eV.

The fundamental quantity expressing the thermodynamic stability of an alloy is the formation energy. For the compound Ti_3Nb the energy of formation ΔE is defined by the difference of corresponding DFT total energies E, according to

$$\Delta E = \frac{1}{4}\left\{E(\mathrm{Ti_3Nb}) - 3E(\mathrm{Ti}) - E(\mathrm{Nb})\right\}. \qquad (1)$$

All formation energies of our studies are given in units of eV atoms^{-1}. The reference energies for the pure states where calculated for the solid phases of hcp Ti and bcc Nb.

For calculations of the vibrational frequencies of a system we utilized density functional perturbation theory approach, which is implemented in VASP. The supercells used were constructed by multiplying the primitive cell two times along the primitive lattice vectors, resulting in a 32 atoms supercell in the case of G1 structure. The test performed with a larger supercell (three times the primitive cell in all directions, 108 atoms) showed that the phonon frequencies differ only little and the free energy is converged with respect to supercell size. The *PHONOPY* [10] package was used to visualize calculated phonon dispersions. The vibrational contribution to the free energy $F_{vib}(V,T)$ is calculated using the phonon density of states $g(\omega)$ as

$$F_{vib}(V,T) = \int_0^\infty g(\omega)\left[\frac{\hbar\omega}{2} + k_B T \ln(1 - e^{-\hbar\omega/k_B T})\right]. \qquad (2)$$

The electronic contribution to the free energy $F_{el}(V,T)$ is evaluted directly in VASP, by using the Fermi-Dirac function for the smearing of the k-point grid. The electronic contribution is obtained by setting appropriate width of the smearing σ ($\sigma = k_B T$) and calculating the total energy difference with respect the calculation with $\sigma = 0$. The Helmholtz free energy was then calculated by

$$F(V,T) = E(V) + F_{el}(V,T) + F_{vib}(V,T), \qquad (3)$$

where $E(V)$ is the static lattice energy evaluted using Eq. 1. Notice that a weak anharmonicity connected with thermal expansion of the volume V has been omitted in our calculation, because it would make the calculations very time-demanding. The calculations were done at the calculated lattice constants of respective phase. We will showed that stronger anharmonic effects associated with the interaction between phonons must be included in order to describe the stabilization of the cubic G1 phase.

The anharmonic effects were included by means of self consistent ab initio lattice dynamical method (SCAILD). [11] The SCAILD method is an extension of the frozen phonon approach. The method combines the idea of Born's self-consistent phonon approach with accurate ab initio calculations of interatomic forces. All phonons with wave vectors commensurate with the supercell are excited together in the same cell. Due to the simultaneuos presence of all commensurate phonons, the interaction between different lattice vibrations is taken into account. The phonon frequencies are calculated in self-consistent manner by alternating between DFT calculation of Hellman-Feymann forces acting on displaced atoms, and calculating new phonon frequencies and new displacements. The self-consistent loop represents much larger computational effort compared to usual phonon calculation, because the forces have to calculated at each iteration. In our calculations, about 100 iterations were necessary to obtain converged phonon frequencies. Notice that in present calculation anharmonic effects associated with thermal expansion have not been taken into account and the calculations have been performed using the calculated lattice constants. A more detailed description of the SCAILD method can be found in Appendix.

RESULTS

Ground-state stability

The β phase of Ti-Nb alloys undergoes a martensitic transformation to a hexagonal structure at low temperatures. According to the phase diagram the martensitic temperature decreases with increasing Nb content, but the chemical decoration -positions of Nb atoms- of the alloys is still unknown. For high temperature β phase, we follow recent study by Nagasako et al. [5], who performed supercell based search over many different possible distributions of Ti and Nb atoms in the

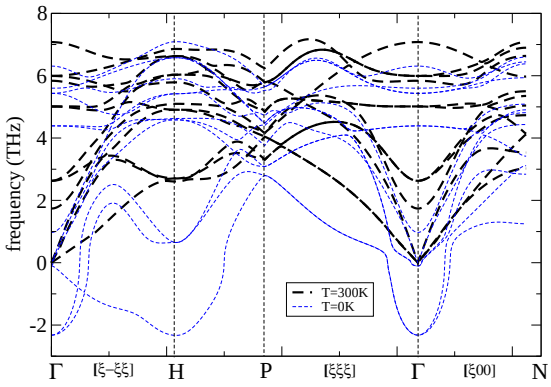

FIG. 1: The phonon dispersions of G1-Ti_3Nb calculated at T=0 K (density functional perturbation theory calculation, blue dashed lines) and T=300 K (SCAILD calculation, black dashed lines).

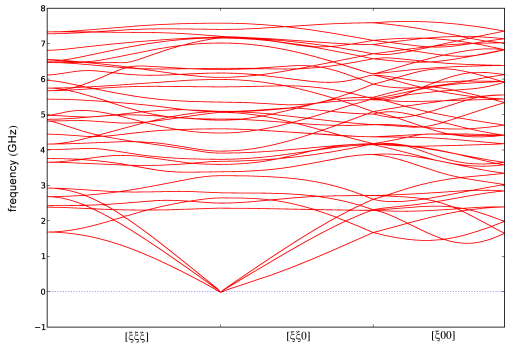

FIG. 2: The phonon dispersions of stable hexagonal Ti_3Nb phase calculated by density functional perturbation theory approach, corresponding to T=0K.

B32 lattice, using a supercell containing 16 atoms. According to their search, there exists a group of 16 symmetry equivalent structures which are energetically the most favorable. Nagasako et al. [5] have called these structures G1-type, and revealed characteristic nearest-neighbor Nb-Nb chain along the body diagonal of the B32 lattice. It should be noted, that for all configurations of Ti and Nb atoms a relaxation of volume and shape of the supercell has been performed. Performing complete relaxation (i.e. including the relaxation of individual atomic positions) leads lattice distortions which destroy cubic symmetry and consequently to a different order of chemical decorations. However, we are interested in a phase with cubic symmetry and, therefore, in following calculations we consider the G1-type lattice as a high temperature cubic phase.

The low temperature hexagonal phase has not been studied in detail so far. Searching for a stable hexagonal Ti-Nb phase of A_3B stoichiometry, we adopted an approach of Nagasako et al. [5]. We constructed a supercell based on a hexagonal B_h lattice and performed simulations for different possible distributions of Ti and Nb atoms in the supercell. To reduce number of possible configurations, the occupation of one half of Ti lattice sites has been fixed, which creates 66 different decorations of the basic B_h structure. For this low temperature phase, we have performed a complete relaxation of the volume and shape of the supercell and also of all atomic coordinates. According to their energies, the structures can be arranged into seven groups and for three of these groups the total energy is lower than for the high temperature cubic G1 phase. The first group contains 24 structures with monoclinically distorted cell and a strong Nb-Nb interaction. These structures are by 15 meV per atom energetically more favorable than the G1 phase. The second group consisting of four structures is by about 3 meV per atom higher in energy than the structures from the first group. The decorations from the second group are closely related to those from the first group, but differ in the absence of the nearest-neighbor Nb-Nb interaction. The third group of structures is still by about 2.5 meV per atom more favorable than the G1 structure and has a nearly tetragonal unit cell. Notice that the presence of a tetragonal phase in 25 and 21.7% Nb alloys was reported [12, 13], however, the identification of this phase was uncertain. The other groups of structures have higher energy than the G1 structure and therefore are not suitable candidates for a martensitic phase. It should be noted that the hexagonal symmetry is perserved only for six structures which are by 17 meV per atom less favorable than the cubic G1 phase.

The α'' martensite has an orthorhombic lattice, which may be viewed as a transition from the hcp structure to the bcc structure of β phase. The space group is Cmcm and the atom positions are $(0,0,0)$, $(1/2,1/2,0)$, $(0,1-2y,1/2)$, and $(1/2,1/2-2y,1/2)$ with y being ≈ 0.1 according to our calculation. The complete relaxation of the orthorhombic cell yields the lattice parameters of 3.34, 4.77, and 4,41 $\mathring{A}$, in a good agreement with those calculated by Sun et al. [14] According to our calculation, the internal energy of α'' is by 20 meV per atom lower than that of the G1 structure and also lower than any of structures based on hexagonal B_h lattice. The stability of α'' is consistent with experimental observations, which reported the occurence of the $\beta \rightarrow \alpha''$ transformation in the Ti-Nb alloys. [15]

Dynamical stability

Fig. 1 shows the calculated phonon dispersions for cubic G1 structure of Ti_3Nb. The density functional perturbation theory calculation (which corresponds to T=0 K) shows imaginary frequencies of some optical phonon branches, indicating that the G1 structure is dynamically unstable for some of optical phonon modes with wave vectors close to Γ-point. On the other hand, real eigen-frequencies are found for all acoustic modes, in agreement with recent study by Nagasako et al. [5], which demostrated that the G1 structure is elastically

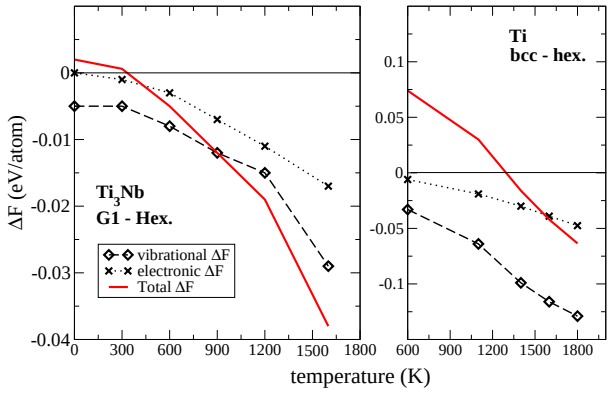

FIG. 3: The free energy differences (red line) between cubic and hexagonal phases of Ti_3Nb and Ti. The differences of vibrational (diamonds) and electronic (crosses) contributions to the free energy are also displayed.

stable. According to Fig. 1, anharmonic effects introduced by the SCAILD calculation stabilize the G1 structure already at room temperature (T=300 K), demostrating that the interaction between different phonon modes provides the main driving mechanism for the stabilization of the G1 structure.

The stabilization of the G1 structure at room temperature justifies recent study by Nagasako et al. [5], which showed that the elastic shear constants of the G1-type Ti_3Nb alloy are very similar to those measured for Gum Metal and consequently assumed that the ordered binary alloy of the G1-type is a good model system for studying the intrinsic properties of Gum Metal. It also worth of notice that the DO_3 structure, which has been used as an approximant for studying binary Gum Metal, is dynamically unstable from $T = O$ K up to $T = 1200$ K according to our perturbation theory and SCAILD calculations. Imaginary acoustic phonon modes occur over large regions of the Brillouin zone and can not be stabilized by phonon-phonon iteractions. This evidence that the DO_3 structure is inadequate for modeling binary Gum Metal supports recent finding, that it is unstable against shear deformations and the formation of vacancies and anti-site point defects. [5] The DO_3 structure is closely related to the structures of the G1-type, but differs in the absence of the nearest-neighbor Nb-Nb interaction.

For the low temperature hexagonal Ti_3Nb phase, we used density functional perturbation theory approach, because we search for a structure dynamically stable already at low temperatures, i.e. we do not consider if a structure is evetually stabilized by phonon-phonon interactions at elevated temperatures. We calculated the phonon dispersions of all structures with internal energy higher than that of the G1 structure, because the most of derived hexagonal chemical decorations showed imaginary frequencies. Thus, we had to find the dynamically stable pattern with the lowest possible total energy. According to our perturbation theory calculation, all 24 chemical decorations contained in the energetically most favorable first group are dynamically unstable, displaying imaginary phonon frequencies along the Γ-$[\xi\xi 0]$ wave vector. The favorable and dynamically stable structures were found in the second group and their phonon dispersions are shown in Fig. 2. These structures are closely related to the structures from the first group, being monoclinically distorted hexagonal structures, and are by 0.007 eV/atom more favorable than the G1 structure.

Figure 3 shows calculated Helmholtz free energy as a function of temperature for stable low temperature Ti_3Nb phase and cubic G1 structure. The transformation to cubic phase appears around $T_k = 500$ K. We also calculated the hexagonal-cubic transformation in pure Ti for the reference and displayed its free energy in the right panel of Fig. 3. Obviously, martensitic transformation from hexagonal to cubic phase appears at much lower temperature in Ti_3Nb compared to Ti. Notice, that pure Nb crystallizes in cubic bcc structure, and Nb content in Ti-Nb alloys influences the temperature of martensitic transformation according to experiments. This fact is well reflected in our calculation, when one compares calculated transition temperatures of Ti and Ti_3Nb. The free energy differences displayed in Fig. 3 arise from the self-consistent SCAILD calculation for the cubic phase and harmonic calculation for the low temperature phase. Wondering how the different methods used for phonon calculation influenced the free energy, we performed test calculation for the bcc Ti and the G1 structure using a harmonic approximation. According to this calculation, anharmonic effects bring negligible contribution to the vibrational free energy at ambient temperatures and become relevant at temperatures higher than 1000 K, thus calculated transition temperatures are barely influenced.

According to our calculation, martensitic tranformation in Ti should appear around 1300K, which corresponds very well to experimental results reporting T_k around 1155K for Ti. One has to consider that the transition temperature is very sensitive to the energy difference between the hcp and bcc phase of Ti. The static energy difference between the cubic and hexagonal phase of Ti is 114 meV/atom according to our calculation. Notice that for the calculation of $F_{vib}(V,T)$ of bcc Ti we have used the the lattice parameter calculated by volume relaxation at $T = 0K$. In order to investigate the influence of thermal expansion we evaluated the total free energy $F(V,T)$ for several volumes V at the temperature T=1200K, which is close to the experimental transition temperature. A reduction of $F(V,T)$ by 12 meV was found, which would decrease the calculated transition temperature by ≈ 120 K, giving the transition temperature of Ti in almost perfect agreement with experiment.

For understanding of strength-limiting mechanisms and deformation behavior in Gum Metal is important to reveal the occurence of the stress-induced martensitic transformation to the orthorhombic α'' phase that is found in a number of Ti alloys. The orthorhombic lattice of α'' martensite is dynamically stable, which is demonstrated by real eigenvalues of the phonon frequencies in Fig. 4. Observing Fig. 5, which dis-

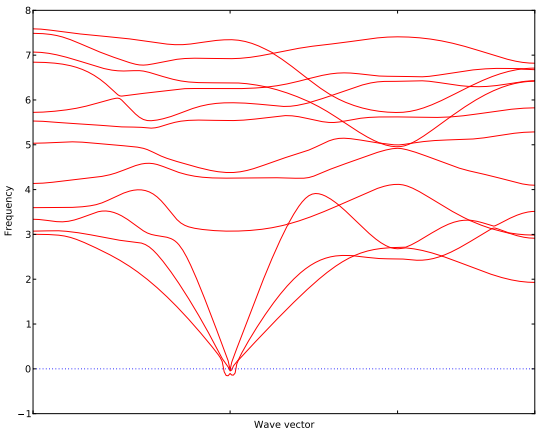

FIG. 4: The phonon dispersions of orthorhombic α'' martensite of Ti_3Nb calculated by density functional perturbation theory approach, corresponding to T=0K.

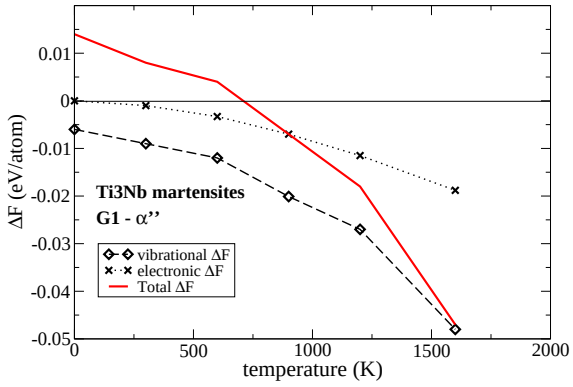

FIG. 5: The free energy differences between cubic G1 and orthorhombic α'' martensite in Ti_3Nb. The differences of vibrational and electronic contributions to the free energy are also displayed.

plays the free energy differences between cubic G1 and orthorhombic α'' martensite in Ti_3Nb, one realizes that α'' has a rather large region of stability at low temperatures and martensitic temperature is around 600 K. The α'' phase is more stable that hexagonal low temperature structure and its stability arises mainly from large difference in internal energies of the G1 and α'' structures. Notice also that vibrational as well as electronic contributions to the free energy are relevant for the stabilization of the G1 phase.

The calculated martensitic temperature of 600 K is somewhat higher than martensitic temperatures measured for Gum Metal, which are reported around 300-400K (see Ref. 15 and references therein), depending on the composition of the alloy and technology used for its production. Large region of α'' stability in pure Ti-Nb system agrees with recent experimental study, which concluded that oxygen stabilizes the β phase. The greater oxygen content increases the material's resistance to the α'' transformation by increasing the magnitude of the shear elastic constant C', which is associted with the $\beta \rightarrow \alpha''$ transformation. [16] The experiments also indicate that a critical amount of prior deformation is required to trigger the transformation. [17]

CONCLUSIONS

First, we focused on model systems for high temperature austenite phase in Ti_3Nb. The phonon spectra within the harmonic approximation of recently proposed G1-type structure, [5] is dynamically unstable for some of optical phonon modes with wave vectors close to γ-point. On the other hand, real eigen-frequencies are found for all acoustic modes, in agreement with the study by Nagasako et al. [5], which demostrated that the G1 structure is elastically stable. We showed that anharmonic phonon-phonon interactions introduced by means of the self-consistent SCAILD scheme stabilize the G1 structure already at room temperature (T=300 K). We also inspected the DO_3 structure, which has been often used as an approximant for studying binary Gum Metal, and found that it is dynamically unstable from $T = Ok$ up to $T = 1200K$ and anharmonic effects in SCAILD scheme are not sufficient to stabilize the DO_3 structure.

We evaluted relative stability of many hexagonal structures by performing a search over different possible distributions of Ti and Nb atoms in a hexagonal B_h lattice. We found a group of monoclinically distorted hexagonal structures, which are 1) by 0.007 eV/atom energetically more favorable than the G1 structure of β phase and 2) dynamically stable, showing real phonon eigenfrequencies in all directions. The martensitic temperature of $\approx$ 400 K was calculated for this martensite phase. Comparing martensitic transformations from hexagonal to cubic phase in Ti_3Nb to Ti, we demonstrated that Nb atoms significantly lower the martensitic temperature in agreement with experimental observations of the role of Nb content in Ti-Nb alloys. [15]

In the case of orthorhombic α'' martensite we relaxed lattice parameters of the structure described in the literature [6]. The complete relaxation of the orthorhomboc cell yields the lattice parameters of 3.34, 4.77, and 4,41 $\AA$, in a good agreement with those calculated by Sun et al. [14] According to our calculation within harmonic approximation, the orthorhombic lattice of α'' martensite is dynamically stable. The α'' has a rather large region of stability at low temperatures and martensitic temperature is around 600 K. The α'' phase is more stable that hexagonal low temperature structure and its stability arises mainly from large difference in internal energies of the G1 and α'' structures. Our calculations also showed that though the vibrational contribution to the free energy is dominant for the stabilization of the G1 phase, electronic contribution are not negligible and must be considered in calculations. Large region of α'' stability in pure Ti-Nb system agrees

with recent experimental study, which concluded that oxygen present in Gum Metal type alloys increases the resistance to α'' transformation and stabilizes the cubic β phase. [17]

APPENDIX

The SCAILD method is based on the calculation of Hellman-Feynmann forces acting on atoms in a supercell. All phonons with wave vectors **q** commensurate with the supercell are excited by displacing atoms situated at the undistorted positions **R** + $\mathbf{b}_j$ to new positions **R** + $\mathbf{b}_j$ + $\mathbf{U}_{\mathbf{R}j}$, where the displacements are given by

$$\mathbf{U}_{\mathbf{R}j} = \frac{1}{\sqrt{N}} \sum_{\mathbf{q}s} A^j_{\mathbf{q}s} \epsilon^j_{\mathbf{q}s} \exp^{i\mathbf{q}(\mathbf{R}+\mathbf{b}_j)} . \tag{4}$$

Here **R** represents the N Bravais lattice sites of the supercell, $\mathbf{b}_j$ the position of atom j relative to its site, $\epsilon^j_{\mathbf{q}s}$ are the phonon eigenvectors corresponding to the phonon mode s. The mode amplitude $A^j_{\mathbf{q}s}$ can be calculated from the different phonon frequencies $\omega_{\mathbf{q}s}$ as

$$A^j_{\mathbf{q}s} = \pm \sqrt{\frac{\hbar}{2M_j\omega_{\mathbf{q}s}} \coth\left(\frac{\hbar\omega_{\mathbf{q}s}}{2k_BT}\right)}, \tag{5}$$

in which T the temperature of the system and M_j the mass of atom j. The phonon frequencies $\omega_{\mathbf{q}s}$ appearing in this expression can be obtained from the Fourier transform $\mathbf{F}^j_{\mathbf{q}}$ of the forces acting on the atoms in the supercell by

$$\omega_{\mathbf{q}s} = \sqrt{-\sum_j \frac{\epsilon^j_{\mathbf{q}s}\mathbf{F}^j_{\mathbf{q}}}{A^j_{\mathbf{q}s}M_j}}. \tag{6}$$

In the SCAILD scheme the equations are solved first by calculating a starting guess for the phonon dispersions by means of standart supercell calculation using direct-displacement method [**?**]. The phonon frequencies corresponding to **k**-vectors commensurate with the supercell are then used to calculate the atomic displacements through Eq. 4, Eq. 5, and Eq. 6. The forces induced by the displacements $\mathbf{U}_{\mathbf{R}j}$ are calculated by the VASP code. From the Fourier transform of new forces a set of frequencies is calculated using Eq. 6. The mean value of all iterations provides a new set of frequencies

$$\omega_{\mathbf{q}s}(N_i) = \frac{1}{\sqrt{N_i}} \sqrt{\sum_{i=1}^{N_i} \Omega^2_{\mathbf{q}s}(i)}, \tag{7}$$

where $\Omega_{\mathbf{q}s}(i)$ are the frequencies restored from previous iterations. These steps are repeated until convergency is reached. In our calculations, about 100 iterations were necessary to obtain converged phonon frequencies, which makes SCAILD calculation considerably more expensive than usual direct-displacement or density functional perturbation phonon calculation. Anharmonicities associated with thermal expansion of the lattice are not included in SCAILD scheme, but may be taken into account by performing SCAILD calculation at several diferent volumes of the cell.

[1] T. Saito, T. F. nad J. H. Hwang, S. Kuramoto, K. Nishino, N. Suzuki, R. Chen, A. Yamada, K. Ito, H. Ikehata, N. Nagasako, et al., Science **300**, 46 (2003).

[2] T. Li, J. W. Morris, N. Nagasako, S. Kuramoto, and D. C. Chrzan, Phys. Rev. Lett. **98**, 105503 (2007).

[3] R. J. Talling, R. J. Dashwood, M. Jackson, S. Kuramato, and D. Dye, Scr. Mater. **59**, 669 (2008).

[4] Y. Yang, G. P. Li, G. M. Cheng, Y. L. Li, and K. Yang, Appl. Phys. Lett. **94**, 061901 (2009).

[5] N. Nagasako, M. Jahnatek, R. Asahi, and J. Hafner (2010).

[6] D. L. Moffat and D. C. Larbalestier, Metall. Trans. A **19**, 1677 (1988).

[7] P. E. Blöchl, Phys. Rev. B **50**, 17953 (1994).

[8] G. Kresse and D. Joubert, Phys. Rev. B **59**, 1758 (1999).

[9] J. P. Perdew and Y. Wang, Phys. Rev. B **45**, 13244 (1992).

[10] A. Togo, F. Oba, and I. Tanaka, Phys. rev. B **78**, 134106 (2008).

[11] P. Souvatzis, O. Eriksson, M. I. Katsnelson, and S. P. Rudin, Phys. Rev. Lett. **100**, 095901 (2008).

[12] B. A. Hatt and V. G. Rivlin, Brit. J. Appl. Phys. **1**, 1145 (1968).

[13] D. Pattanayak, B. Obst, and U. Wolfsteig, Z. Metall. **72**, 481 (1981).

[14] J. Sun, Q. Yao, H. Xing, and W. Y. Guo, Journal of Physics: Condensed Matter **19**, 486215 (2007).

[15] H. Y. Kim, Y. Ikehara, J. I. Kim, H. Hosoda, and S. Miyazaki, Acta Mater. **54**, 2419 (2006).

[16] R. J. Talling, R. J. Dashwood, M. Jackson, and D. Dye, Scr. Mater. **60**, 1000 (2009).

[17] R. J. Talling, R. J. Dashwood, M. Jackson, and D. Dye, Acta Materialia **57**, 1188 (2009).